Journal of Inorganic and General Chemistry
ZAAC
Zeitschrift für anorganische und allgemeine Chemie
DOI: 10.1002/zaac.201900204
ARTICLE

Synthesis and Upconversion Luminescence in LaF_3:Yb^{3+}, Ho^{3+}, GdF_3: Yb^{3+}, Tm^{3+} and YF_3:Yb^{3+}, Er^{3+} obtained from Sulfide Precursors

Illariia A. Razumkova,*[a] Yuriy G. Denisenko,[a,b] Andrey N. Boyko,[a] Denis A. Ikonnikov,[c] Aleksandr S. Aleksandrovsky,[c,d] Nikita O. Azarapin,[a] and Oleg V. Andreev[a]

Abstract. Rare earth fluorides are mainly obtained from aqueous solutions of oxygen-containing precursors. Probably, this method is simple and efficient, however, oxygen may partially be retained in the fluoride structure. We offer an alternative method: obtaining fluorides and solid solutions based on them from an oxygen-free precursor. As starting materials, we choose sulfides of rare-earth elements and solid solutions based on them. The fluorination is carried out by exposure to hydrofluoric acid of various concentrations. The transmission electron microscopy images revealed the different morphologies of the products, which depend on the concentration of the fluorinating component (HF) and the host element. The solid solution particle size varied from 30–35 nm in the case of GdF_3:Yb^{3+}, Tm^{3+} (4 % HF) to larger structures with dimensions exceeding 200 nm, such as that for LaF_3:Yb^{3+}, Ho^{3+} (40 % HF). The thermal characteristics, such as the temperatures of the transitions and melting and enthalpies, were determined for the solid solutions and simple fluorides. Applicability of the materials obtained as biological luminescent markers was tested on the example of upconversion luminescence, and good upconversion properties were detected.

Introduction

Photodynamic therapy is one of the effective methods for oncological treatment that does not harm the body.[1–3] Fluorides of rare earth element (REF_3) can potentially be used as biomarkers owing to their chemical resistance.[4,5] Among the known materials, the most promising crystals are $NaYF_4$, YF_3, LaF_3, and GdF_3, which are doped with a pair of rare-earth elements strictly determined by the high light conversion activity the pair, with the excitation region at the wavelength in the tissue transparency region.[6,7] In addition, the REF_3 compounds are promising as luminescent and optical materials.[8–12]

Fluorides of rare earth elements exhibit characteristic morphotropic behavior.[13,14] These compounds crystallize in four different groups: (1) fluorides of La – Nd crystallize in the tysonite (LaF_3) structure type (trigonal crystal system, space group $P\bar{3}c1$; (2) fluorides of Sm – Gd crystallize in the low-temperature modification of the β-YF_3 structural type (orthorhombic crystal system, space group *Pnma*) and in the high-temperature modification of tysonite;[15,16] (3) throughout the temperature access, fluorides of Tb – Ho crystallize only in the structural type β-YF_3; and (4) fluorides of Er – Lu, Y crystallize both in the basic orthorhombic modification (β-YF_3) and high-temperature α-YF_3 (trigonal crystal system, space group $P\bar{3}m1$).[17]

For the rare earth elements of the yttrium subgroup, a compound with the δ-$(H_3O)RE_3F_{10}{\cdot}nH_2O$ structure is known. The compounds δ-$(H_3O)RE_3F_{10}{\cdot}nH_2O$ crystallize in a cubic crystal system with the diamond type structure composed of the $[RE_6F_{32}]^{-14}$ octahedral blocks constructed from the REF_8 square antiprisms.[18,19] In the structure, both zeolite behavior of the water molecules and cation-exchange properties are observed.[20] The compounds δ-$(H_3O)RE_3F_{10}{\cdot}nH_2O$ were obtained in the course of hydrothermal synthesis during the reaction of lanthanide oxalates (Er – Lu, Y) with hydrofluoric acid,[21] and a secondary phase was obtained with the interaction of a solution of nitrates of yttrium and alkaline earth metal (strontium,[22] barium[23]) with hydrofluoric acid (47 %). The diamond-structure compounds[19,24] are formed for rare-earth elements from holmium ($r{Ho^{3+}}_{(CN\ 8)}$ = 1.155 Å[25]) to lutetium ($r{Lu^{3+}}_{(CN\ 8)}$ = 1.117 Å[25]), Y: $ARE_3F_{10}{\cdot}nH_2O$ (A^+ = K^+, Rb^+, NH_4^+, Cs^+),[21] $(C_2N_2H_{10})_{0.5}RE_3F_{10}{\cdot}nH_2O$,[26] $(C_3N_2H_{12})_{0.5}RE_3F_{10}{\cdot}nH_2O$.[27]

The methods for obtaining fluorides of rare earth elements can be divided into precipitation,[28,29] hydrothermal,[30,31] micro-emulsion[32,33] and microwave[34] thermal decomposition[35] techniques. The synthesis of nanofluoride *RE*s is mainly realized by pyrolysis of fluorine-containing precursors,

* I. A. Razumkova
Fax: +73452597559
E-Mail: razumkova@list.ru
[a] Department of Inorganic and Physical Chemistry
Tyumen State University
6, Volodarskogo Street
Tyumen, 625003, Russia
[b] Department of General and Special Chemistry
Industrial University of Tyumen
38, Volodarskogo Street
Tyumen, 625000, Russia
[c] Laboratory of Coherent Optics
Kirensky Institute of Physics Federal Research Center KSC SB RAS
Krasnoyarsk 660036, Russia
[d] Department of Photonics and Laser Technology
Siberian Federal University
Krasnoyarsk 660041, Russia
Supporting information for this article is available on the WWW under **http://dx.doi.org/10.1002/zaac.201900204** or from the author.

hydrothermal synthesis, micro-emulsion method, solvothermal synthesis and the sol-gel method.[36–38]

REF_3 and $NaYF_4$ were obtaining from sulfide precursors via the reaction with hydrofluoric acid.[39–41] The fluorides of rare earth elements obtained by this method do not contain *RE*OF.[42,43] The synthesis of high-purity *RE*F_3 samples allows them to be used for the determination of the thermal characteristics of *RE*F_3 compounds and solid solutions based on them.

The temperatures and enthalpies of melting of *RE*F_3, when fluorinated with RE_2O_3 by gaseous HF at 750 °C and subsequent fluorination in the melt, were studied by a calorimetric method.[44,45] The thermal characteristics of *RE*F_3 compounds by the differential scanning calorimetry method associated with thermogravimetric analysis have not been found in the literature.

The present work is devoted to the solid solutions *RE*F_3:10 %Yb^{3+},5 %RE'^{3+} (*RE* = La, Gd, Y, *RE'* = Ho, Tm, Er) obtained through the oxide and sulfide precursors and it is aimed at the study of the thermal characteristics of *RE*F_3 compounds and their solid solutions.

Experimental Section

Materials: The synthesis was carried out using commercially available reagents. Ultrapure 99.999 wt.-% RE_2O_3 was supplied by Uralredmed (Pyshma, Russia), and 99.99 wt.-% HNO_3 with concentration 67 % was supplied by Vekton (St. Petersburg, Russia). NH_4SCN was 98.5 wt.-%, and HF was 99.9 wt.-% with concentration 40 %; both were provided by Sigma TEK (Moskow, Russia). To decompose the hydroxides and carbonates formed during storage, the starting oxides RE_2O_3 (*RE* = La, Gd, Y, Ho, Er, Yb) were calcined in the air in corundum crucibles in a muffle furnace at 900 °C.

Caution to Synthesis! Carbon disulfide and hydrofluoric acid, which used in the synthesis, are toxic. The experiments using carbon disulfide and hydrofluoric acid are required in fume hoods, and personal protective equipment should be used.

Synthesis of *RE*F_3 (*RE* = La, Gd, Y): The *RE*F_3 samples were obtained in accordance with the standard procedures[46,47] using RE_2S_3 sulfides with a 10-fold excess of hydrofluoric acid aqueous solution HF (40 %). The precipitates of the *RE*F_3 compounds were separated from the solution by decanting, followed by washing with distilled water to pH = 6.6. The neutral *RE*F_3 powders were dried at 100 °C in air for 5 h, followed by annealing at 700 °C for 30 min in fluoropolymer decomposition vapor.[40]

Synthesis of RE_2O_3:10 %Yb^{3+}, 5 %RE'^{3+} (*RE* = La, Gd, Y; *RE'* = Ho, Tm, Er): The oxide masses (2 g) in the stoichiometric ratio (85:10:5) were dissolved in a small excess of nitric acid (5 mL). The nitrate mixture solution was thermally decomposed at 1000 °C in a quartz glass and held for 4 h at this temperature to form a solid solution of oxides.

Synthesis of RE_2S_3:10 %Yb^{3+}, 5 %RE'^{3+} (*RE* = La, Gd, Y; *RE'* = Ho, Tm, Er): Complex oxide weighing up to 5 g was placed in a optical quartz reactor. A mixture of sulfiding gases (CS_2 and H_2S) was passed through the complex oxide powder. Hydrogen sulfide and carbon disulfide are obtained as a result of thermal decomposition of ammonium thiocyanate at 250–300 °C. The feed rate of sulfiding gases was 20–25 mL·h^{-1}. The rate was regulated by a carrier gas for which argon was used (purity 99.999 %). The synthesis of complex sulfides RE_2S_3:Yb^{3+},RE'^{3+} was carried out at 1000–1050 °C for 5 h.

Synthesis of *RE*F_3:10 %Yb^{3+}, 5 %RE'^{3+} (*RE* = La, Gd, Y; *RE'* = Ho, Tm, Er): The RE_2S_3:Yb^{3+},RE'^{3+} powders were treated in 10-fold excess of hydrofluoric acid with the concentration of 4 % or 40 %. All experiments were held in a glass graphite crucible at ambient temperature (21–25 °C). The resulting precipitate was decanted, washed thoroughly with distilled water and dried in a sand heated bath at 60 °C for 2–3 h. The sand heated bath consisted of dried fine river sand and ammonium fluoride (100:1). The ammonia and hydrogen fluorides formed in the process of dissociation ensure the creation of a reducing-fluorinating atmosphere above the bath, which prevents the oxidation and pyrohydrolysis of the dried fluorides.

Characterization: The chemical composition of the samples was determined by X-ray spectroscopy using a scanning electron microscope JSM-6510LV, (JEOL, Japan) with the accelerating voltage of 20 kV.

The X-ray diffraction (XRD) patterns were measured with a DRON 7 X-ray diffractometer using Cu-K_α radiation (λ = 1.541874 Å) in the 2Θ range of 10° to 90°. The cell parameters calculated in the PowderCell software package and refined using a survey with a reference (crystalline silicon). The density of the powders was determined using a standard pycnometer. Toluene was used as a working liquid, in which the particles are not dissolved. The measurements were carried out under vacuum with a residual pressure of 10^{-2} Pa.

Thermal analysis was performed using a synchronous thermal analyser STA 449 F3 MOMQ-1000D (NETZSCH, Germany) (corundum crucibles, argon, heating rate of 2 °·min^{-1}, sample weight of approximately 25 mg). The DSC/TG measurements were taken on an NETZSCH STA 449 F3 Jupiter simultaneous thermal analyser. The measurements were taken under the helium (99.99999 %) atmosphere at the flow rate of 70 mL·min^{-1} using 100–110 mg samples that were pre-melted in GAZN95 crucibles (NETZSCH, Germany). A linear heating rate of 5 K·min^{-1} was employed. The DSC peak areas were determined with use of the „Proteus 6 2012" program. The thermal analyzer was calibrated by a DTA and DSC calibration set (In, Sn, Bi, Zn, Al, Ag, Au, and Ni). Two replicate measurements were taken for each ReF_3 compound and *RE*F_3:Yb^{3+}, RE'^{3+}. Data processing showed that the compound melting temperature were determined with the accuracy of ± (2–3 °C) and, for the enthalpies of melting, the determination accuracy was ± (3 %). The heat of the phase transformation was determined by averaging the values of the enthalpies of melting in heating and cooling cycles.

Supporting Information (see footnote on the first page of this article): presents individual X-Ray diffraction patterns of solid solutions (RE_2O_3:Yb^{3+}, RE'^{3+}; RE_2S_3:Yb^{3+}, RE'^{3+} and *RE*F_3:Yb^{3+}, RE'^{3+}) processed by the Rietveld refinement.

Results and Discussion

The samples obtained by the thermal decomposition of a mixture of rare-earth nitrates were identified as RE_2O_3:Yb^{3+}, RE'^{3+} solid solutions. The X-ray diffraction patterns of the samples did not show impurity phases in the quantities that can be determined by this method. The RE_2O_3:Yb^{3+}, RE'^{3+} solid solutions crystallize in the crystal structure types of the simple oxides of the host element. For all solid solutions, the obtained cell parameters are smaller than those for the standard host oxide samples that is due to the introduction of ions with

Table 1. Structural characteristics of crystalline samples obtained at 700 °C.

Anion	Cationic mixture 85 % La^{3+} 10 % Yb^{3+} 5 % Ho^{3+}	85 % Gd^{3+} 10 % Yb^{3+} 5 % Tm^{3+}	85 % Y^{3+} 10 % Yb^{3+} 5 % Er^{3+}
O^{2-}	Hexagonal crystal system $P6_3/mmc$ 85–1355 $a_{(exp)}$ = 3.903(2) Å $c_{(exp)}$ = 6.237(2) Å	Cubic crystal system $I2_13$ 76–0155 $a_{(exp)}$ = 10.690(1) Å	Cubic crystal system $Ia3$ 86–1326 $a_{(exp)}$ = 10.550(1) Å
	$a_{(theor)}$ = 3.978(2) Å $c_{(theor)}$ = 6.304(2) Å	$a_{(theor)}$ = 10.691(1) Å	$a_{(theor)}$ = 10.552(1) Å
S^{2-}	Orthorhombic crystal system *Pnma* 73–0957 $a_{(exp)}$ = 7.510(5) Å $b_{(exp)}$ = 15.630(5) Å $c_{(exp)}$ = 4.140(5) Å	Orthorhombic crystal system *Pnma* 76–0265 $a_{(exp)}$ = 7.192(5) Å $b_{(exp)}$ = 14.973(5) Å $c_{(exp)}$ = 3.853(5) Å	Monoclinic crystal system $P2_1/m$ 79–2250b $a_{(exp)}$ = 17.48(1) Å $b_{(exp)}$ = 4.00(1) Å $c_{(exp)}$ = 10.15(1) Å β = 98,69°
	$a_{(theor)}$ = 7.440(5) Å $b_{(theor)}$ = 15.558(5) Å $c_{(theor)}$ = 4.065(5) Å	$a_{(theor)}$ = 7.260(5) Å $b_{(theor)}$ = 15.096(5) Å $c_{(theor)}$ = 3.878(5) Å	$a_{(theor)}$ = 17.46(1) Å $b_{(theor)}$ = 4.00(1) Å $c_{(theor)}$ = 10.13(1) Å β = 98,75°
F^-	Hexagonal crystal system $P\bar{3}c1$ 84–0943 $a_{(exp)}$ = 7.040(2) Å $c_{(exp)}$ = 7.190(2) Å	Orthorhombic crystal system *Pnma* 49–1804 $a_{(exp)}$ = 6.500(5) Å $b_{(exp)}$ = 6.912(5) Å $c_{(exp)}$ = 4.395(5) Å	Orthorhombic crystal system *Pnma* 74–0911 $a_{(exp)}$ = 6.360(5) Å $b_{(exp)}$ = 6.850(5) Å $c_{(exp)}$ = 4.400(5) Å
	$a_{(theor)}$ = 7.092(2) Å $c_{(theor)}$ = 7.255(2) Å	$a_{(theor)}$ = 6.517(5) Å $b_{(theor)}$ = 6.927(5) Å $c_{(theor)}$ = 4.354(5) Å	$a_{(theor)}$ = 6.330(5) Å $b_{(theor)}$ = 6.825(5) Å $c_{(theor)}$ = 4.377(5) Å

a smaller ionic radius into the host structure. The cell parameters of solid solution, calculated theoretically and experimentally determined, are in good relation (Table 1). The Shannon radii for certain types of atom were used for theoretical calculation of the lattice parameters of a unit cell. The calculation was based on the fact that in the process of doping, the crystal system, space group, and coordination number of atoms would not be changed. In addition, we assume the case of formation to be similar with substitutional solid solutions. Subject to these requirements, it is possible to calculate the cell parameters based on the concept, according with which unit cell parameters would be changed proportionally with the proportional substitution of atoms. Theoretical calculation of cell parameters for a monoclinic structure is complicated by a change in the angle β, which depends on changes in the cell parameters a and c. For this reason, the contribution of each element (Er, Yb and Y) was calculated from the calculation of the isostructural parameters of these elements in compounds. The deviation of the theoretical and experimental cell parameters does not exceed 2 %.

The X-ray diffraction patterns of RE_2O_3:Yb^{3+}, RE'^{3+} solid solutions contain relatively broad lines (Figure 1, Figure 2, and Figure 3a). The diffraction peaks could broaden owing to the small size of the crystallites (less 100 nm); alternatively, their broadening indicates the presence of defects in the crystal structure. The broadening of XRD lines is primarily associated with the small size of coherent scattering regions. The average crystallites sizes estimated by the Scherrer equation for all compounds are shown in Table 2.

The SEM study of RE_2O_3:Yb^{3+}, RE'^{3+} powders revealed that all samples consist of individual particles of different shapes depending on the host element [La – spherical particles (Figure 1b), Gd – acicular particles (Figure 2b), and Y – ellipsoidal particles (Figure 3b)]. The high annealing temperature leads to the agglomerate formation. The average diameter and length of particles were determined from the results of 200 measurements. The average diameter and density of the particles are presented in Table 2.

The RE_2S_3:Yb^{3+}, RE'^{3+} powders were obtained as a result of the interaction of RE_2O_3:Yb^{3+}, RE'^{3+} solid solutions with sulfiding agents (H_2S and CS_2). The X-ray diffraction patterns of the samples only have diffraction maxima of a structural type that is inherent to the RE_2S_3 compound. The diffraction peaks of other sulfides [Yb_2S_3 and RE'_2S_3 (Ho, Tm, Er)] are not detected. In the RE_2S_3:Yb^{3+}, RE'^{3+} solid solutions, a decrease in the cell parameters is observed compared to those of the RE_2S_3 compounds. The cell parameters decrease in the solid solutions is consistent with the relations of ionic radii of parent and dopant cations (Table 1). The sulfur and rare-earth elements content in compressed powders were determined by the EDS on the JSM-6510LV. The experimental content matches to the theoretical value in the range of 0.2–0.3 wt.-% (Table 3).

The morphology of the particles La_2S_3:Yb^{3+}, Ho^{3+} powders is represented by distinguishable ellipsoidal particles with the minimum size (width) of approximately 1.3 μm. The particles form friable spherical agglomerates with a distinct layered structure, which are combined likely "chain-branched" struc-

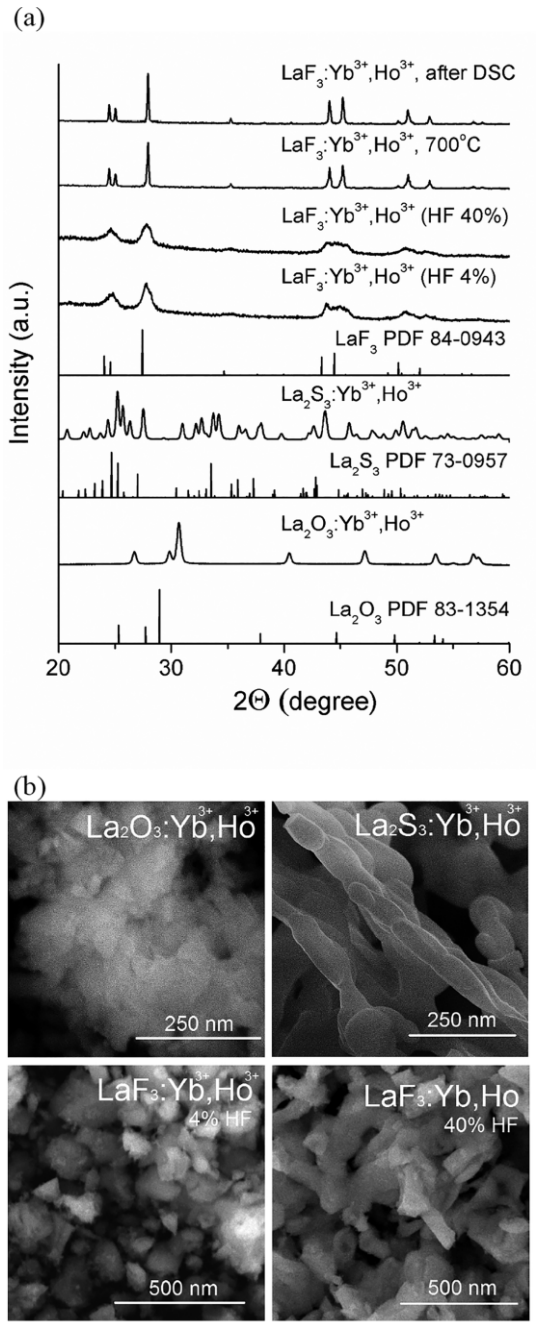

Figure 1. (a) XRD pattern and (b) SEM images of the synthesis steps related to compound LaF_3:Yb^{3+}, Ho^{3+}.

tures with a relief surface and multiple channels (Figure 1b). The Gd_2S_3:Yb^{3+}, Tm^{3+} particles have a regular round shape with a minimum size of 0.5 μm and they form dense agglomerates consisting of three to several dozen particles. Dense agglomerates in turn form loose ellipsoidal conglomerates with a relief surface and multiple channels with the average size of approximately 100 μm (Figure 2b). The smallest distinguishable Y_2S_3:Yb^{3+}, Er^{3+} particles have an ellipsoidal shape with a size of 1.1 μm or 1.5×0.5 μm2, which are combined into "chain-branched" structures with a relief surface and multiple channels. The agglomerates are in the form of separate particles with the maximum size of 70 μm (Figure 3b).

The fluorination of solid solutions RE_2S_3:Yb^{3+}, RE'^{3+} was carried out by hydrofluoric acid at two concentrations: 4 % (pH = 1.9) and 40 % (pH = 0.9). The synthetic route includes treating the sample with a solution of hydrofluoric acid (HF). This potentially can change the ratio of the rare earth elements in the target phase due to the different solubility of the rare earth fluorides. The using of a 10-fold excess of HF allowed avoiding violation of the stoichiometric composition. The retention of the stoichiometric composition RE_2S_3:Yb^{3+}, RE'^{3+} is confirmed by EDS data (Table 3). The contents of fluorine and rare-earth elements in compressed powders are correspondent to theoretically calculated data within the possible error limits of 0.2–0.3 mol %.

The interaction of La_2S_3:Yb^{3+}, Ho^{3+} with hydrofluoric acid of different concentrations leads to the formation of a solid solution of LaF_3:Yb^{3+}, Ho^{3+} of the structural type of tisonite, which is characteristic of LaF_3. In this case, the interaction with 40 % HF leads to the formation of a solid solution with a smaller deviation of the cell parameters in relation to LaF_3. This regularity makes it possible to assume the greatest ordering of ions in the crystal lattice, as well as the most uniform cation vacancy distribution. However, the cell volume, in both cases, is much less than the volume of LaF_3, which correlates with the introduction of smaller radii cations into the lattice of LaF_3. The reflection broadening in the X-ray diffraction patterns (Figure 1a) and the background increase indicate the nanoscale particle formation.

The coherent scattering region values calculated from the Scherrer formula are 45 nm and they do not depend on the concentration of HF. The morphology of solid solution particles is represented by agglomerates of 0.5–3 μm in size (Figure 1b). The size of the individual particles reaches 30×100 nm. The structure of the powder is porous and friable. The results of SEM are consistent with the XRD results.

The GdF_3:Yb^{3+}, Tm^{3+} solid solution with the β-YF_3 type structure is formed by fluorination with hydrofluoric acid at concentrations of 4 and 40 %. This structural type is a characteristic of GdF_3. In contrast to LaF_3:Yb^{3+}, Ho^{3+}, the GdF_3:Yb^{3+}, Tm^{3+} solid solution with the maximum level of ion ordering in the crystal lattice is formed by the reaction of Gd_2S_3:Yb^{3+}, Tm^{3+} with dilute solution of hydrofluoric acid. The X-ray diffraction patterns of the samples are blurry and a low intensity of the reflections is also observed (Figure 2a), which may indicate the nanoscale size of the formed particles. The calculated values of the coherent scattering region are 35–40 nm (4 % HF) and 40–45 nm (40 % HF). The particle morphologies obtained by fluorination with dilute and concentrated hydrofluoric acid are different. The agglomerates with dimensions of 0.2–0.5 μm in the form of stars, consisting of distinct particles with size of 20×70 nm, are formed by fluorination of 4 % HF. The sample also contains individual particles with sizes up to 50 nm. In the sample, there is a clear tendency to reduced aggregation. The particle sizes obtained by two independent methods are in agreement with each other.

Table 2. Average crystallite sizes and powder density.

Compound	Crystallite size /nm		Density /g·cm^{-3}			Compound
	XRD	SEM	ρ (exp.)	ρ (calcd.)	ρ (exp.)	
La_2O_3:Yb^{3+}, Ho^{3+}	–	200	7.01	7.23	5.49	La_2O_3
Gd_2O_3:Yb^{3+}, Tm^{3+}	–	180 × 80	7.90	7.98	7.28	Gd_2O_3
Y_2O_3:Yb^{3+}, Er^{3+}	–	70 × 370	5.53	5.70	4.64	Y_2O_3
La_2S_3:Yb^{3+}, Ho^{3+}	–	1300	4.97	5.24	4.55	La_2S_3
Gd_2S_3:Yb^{3+}, Tm^{3+}	–	500	6.31	6.64	6.01	Gd_2S_3
Y_2S_3:Yb^{3+}, Er^{3+}	–	1100 × 500	4.09	4.26	3.50	Y_2S_3
LaF_3:Yb^{3+}, Ho^{3+}	45	30 × 100	6.29	6.48	5.60	LaF_3
GdF_3:Yb^{3+}, Tm^{3+}	40	20 × 70	7.03	7.36	6.57	GdF_3
YF_3:Yb^{3+}, Er^{3+}	35	30 × 100	5.28	5.51	5.00	YF_3

Table 3. EDS results.

Compound	Cations /wt-%						Anions /wt-%	
	RE (host)		Yb		*RE'* (doped)		S or F	
	exp.	theor.	exp.	theor.	exp.	theor.	exp	theor
La_2S_3:Yb^{3+}, Ho^{3+}	61.58	61.6	9.05	9.0	4.33	4.3	25.04	25.1
Gd_2S_3:Yb^{3+}, Tm^{3+}	64.28	64.4	8.32	8.3	4.13	4.1	23.27	23.2
Y_2S_3:Yb^{3+}, Er^{3+}	50.53	50.6	11.55	11.6	5.62	5.6	32.30	32.2
LaF_3:Yb^{3+}, Ho^{3+}	58.83	58.9	8.57	8.6	4.11	4.1	28.49	28.4
GdF_3:Yb^{3+}, Tm^{3+}	61.87	61.8	8.03	8.0	3.88	3.9	26.22	26.3
YF_3:Yb^{3+}, Er^{3+}	47.73	47.8	10.87	10.9	5.32	5.3	36.08	36.0

For the fluorination with 40 % HF, the morphology of the sample is represented by ellipsoidal particles with the sizes of 0.5–2 μm, and individual particles have sizes up to 0.5 μm (Figure 2b). The sample also contains agglomerates sized 1.5–2 μm, formed from initial subgrains measuring 70 × 100 nm. The enlargement of particles during fluorination with concentrated acid is confirmed by the results of SEM and XRD experiments. This trend is most likely caused by the difference in the pH of the solution and the consequence difference in the reaction rate.

The interaction of the Y_2S_3:Yb^{3+}, Er^{3+} solid solution with 4 % HF leads to the formation of the YF_3:Yb^{3+}, Er^{3+} solid solution crystallized in the β-YF_3 structure (Figure 3a). The cell parameters of the obtained sample show good convergence with theoretically calculated values (Table 1).

According to XRD analysis, the sample obtained by interaction of Y_2S_3:Yb^{3+}, Er^{3+} with 40 % HF is biphasic (Figure 3a). The phase composition of the sample is represented by two solid solutions: a solid solution based on a $(H_3O)Y_3F_{10}{\cdot}H_2O$ compound and a solid solution based on YF_3. The crystallinity of the sample thus bordered on the amorphous state, as evidenced by an overestimated background level and weakly identified reflections. Based on all the available evidence, the mechanism for forming the phase composition of the sample is as follows:

First, when the sulfide solid solution reacts with a concentrated aqueous solution of HF, a solid solution is formed based on the $(H_3O)Y_3F_{10}{\cdot}H_2O$ compound, according to reaction (1) [Equation (1)]. Formation of the $(H_3O)Y_3F_{10}{\cdot}H_2O$ compound is promoted by a significant excess of hydrofluoric acid, which likely causes the protolysis of water and the oxonium ion formation:

$$3\ Y_2S_3{:}Yb^{3+}, Er^{3+} + 20\ HF + 4\ H_2O \rightarrow 2\ (H_3O)Y_3F_{10}{\cdot}H_2O{:}\ Yb^{3+}, Er^{3+} + 9\ H_2S \quad (1)$$

Second, when the $(H_3O)Y_3F_{10}{\cdot}H_2O$ compound is dried, its decomposition proceeds by reaction (2) [Equation (2)]. The low decomposition rate at the drying temperature does not allow completing decomposition and, in turn, leads to the two-phase sample formation. The increase of the heat treatment temperature up to 300 °C or holding time to approximately 7 days leads to the formation of a single-phase sample YF_3:Yb^{3+}, Er^{3+}. The formation and decomposition of compounds in reactions involving fluorides of rare-earth elements of the yttrium subgroup does not contradict modern concepts of the synthetic chemistry of fluoride compounds of rare earth elements:[18,27,48,49]

$$(H_3O)Y_3F_{10}{\cdot}H_2O{:}\ Yb^{3+}, Er^{3+} \rightarrow 3\ YF_3{:}Yb^{3+}, Er^{3+} + 2\ H_2O + HF \quad (2)$$

The SEM study of the YF_3:Yb^{3+}, Er^{3+} powders revealed that all samples were consistent of ellipsoidal particles (Figure 3b) and agglomerates. The average particle diameter is 30 × 100 nm (Table 2). The sample is porous and friable, and the crystallinity of the sample is closer to amorphous. The coherent scattering region values calculated from the Scherrer equation are 35 nm and they are consistent with the SEM results.

LaF_3:Yb^{3+}, Ho^{3+}, GdF_3:Yb^{3+}, Tm^{3+} and YF_3:Yb^{3+}, Er^{3+} there is a preservation of the structural type and an increase to the crystallinity of the samples during thermal annealing at 700 °C for 5–7 minutes in a vacuumed and filled argon reactor. After annealing of the sample obtained by the reaction of Y_2S_3:Yb^{3+}, Er^{3+} with 40 % HF, the compound $(H_3O)Y_3F_{10}{\cdot}H_2O$:$Yb^{3+}$, Er^{3+} is decomposed by reaction (2). The resulting solid solution crystallizes in the β-YF_3 structure.

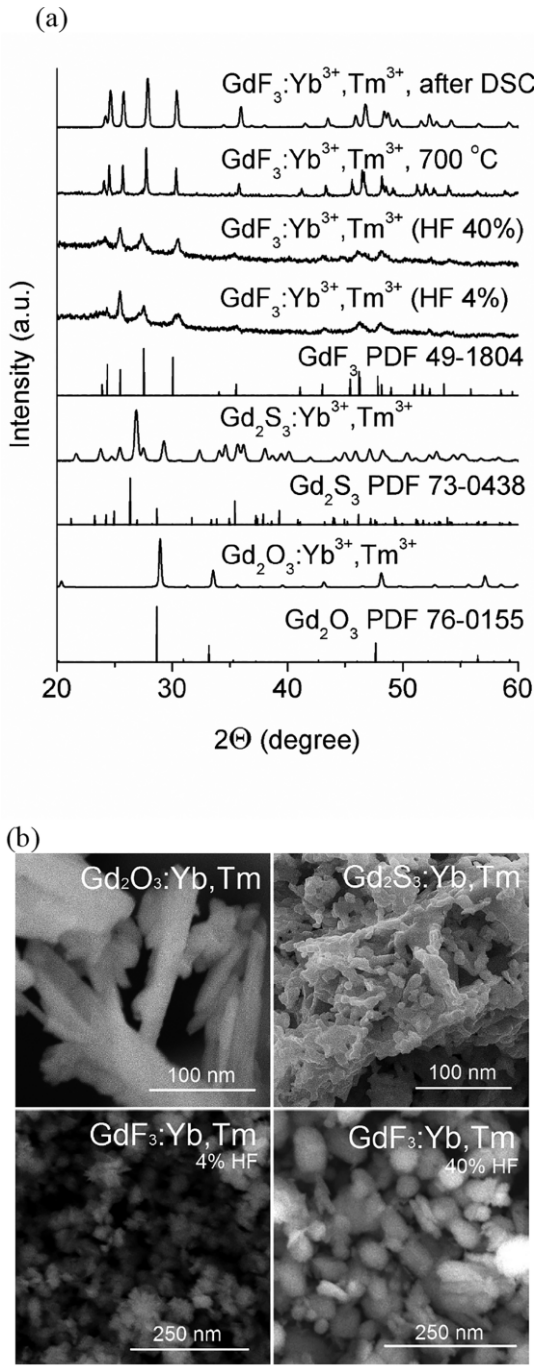

Figure 2. (a) XRD patterns and (b) SEM images of the synthesis steps related to compound GdF_3:Yb^{3+}, Tm^{3+}.

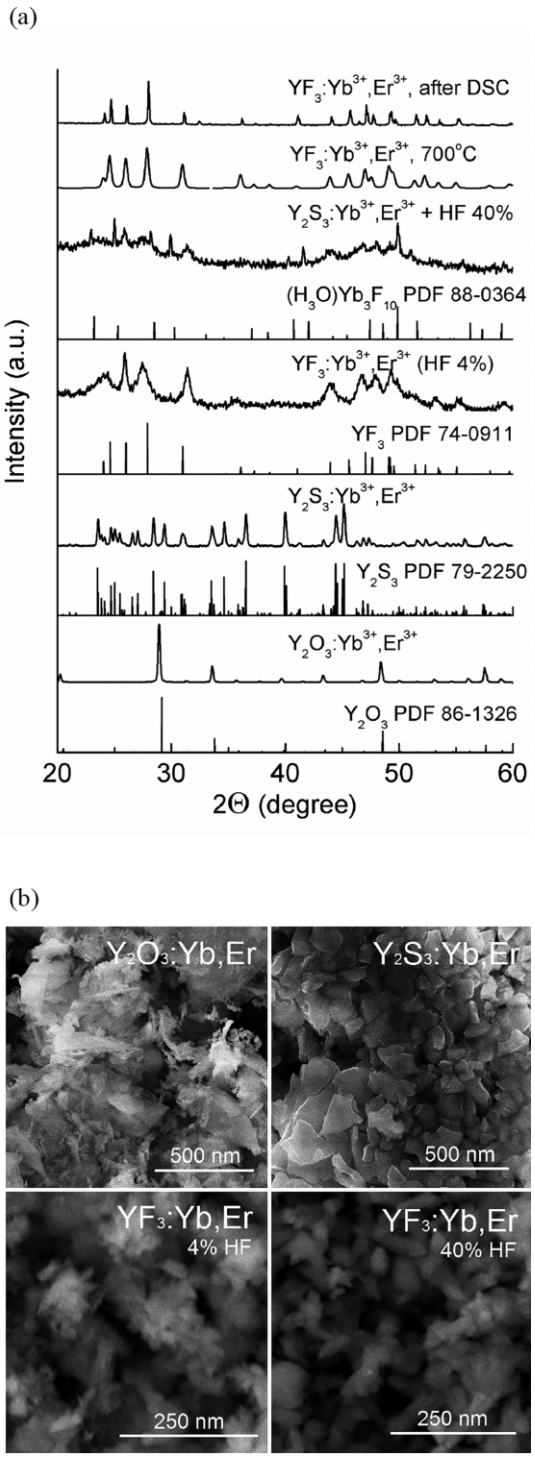

Figure 3. (a) XRD patterns and (b) SEM images related to the synthesis steps for compound YF_3:Yb^{3+}, Er^{3+}.

The fluoride solid solution formation was confirmed by DSC measurements. For comparison, the samples of REF_3 and REF_3:Yb^{3+}, RE'^{3+} were studied. The average temperatures of the beginning of melting and crystallization are shown in Table 4. The REF_3 and REF_3:Yb^{3+}, RE'^{3+} samples melt without mass loss. REF_3 can be easily oxidized to REOF at 700 °C. Each sample was melted two times and the deviation of the characteristic points in the surveys was ±2 °C. In addition, in the X-ray diffraction patterns of the samples after DSC there are no extraneous reflexes.

The established melting points and enthalpies of melting of REF_3 compounds essentially coincide with the previously reported data[14] (Table 4).

Table 4. Temperatures and enthalpies of melting for REF_3 and REF_3:Yb^{3+}, RE'^{3+}.

Compound / Solid solution	Transition				Melting			
	T_{polym} /°C DSC	Cal. [a]	ΔH /kJ·mol^{-1} DSC	Cal. [a]	T_{melt} /°C DSC	Cal. [a]	ΔH /kJ·mol^{-1} DSC	Cal. [a]
LaF_3	–	–	–	–	1498 ± 2	1492	55.2 ± 1.0	50.3
LaF_3:Yb^{3+}, Ho^{3+}	–	–	–	–	1332	–	23.9 ± 0.5	–
GdF_3	1063 ± 2	1070	1.7 ± 0.2	1.3	1233 ± 2	1230	43.0 ± 0.9	50.4
GdF_3:Yb^{3+}, Tm^{3+}	1018 ± 2	–	1.0 ± 0.3	–	1218 ± 2	–	38.5 ± 1.0	–
YF_3	1069 ± 3	1077	29.6 ± 0.6	32.4	1150 ± 0.5	1155	29.3 ± 0.5	28.0
YF_3:Yb^{3+}, Er^{3+}	1045 ± 3	–	24.8 ± 0.5	–	1110 ± 0.5	–	26.3 ± 0.5	–

a) Calorimetry.[14,44,45]

The temperature of transition and melting of GdF_3 depend on the presence of impurity GdOF. The low level content of GdOF in the sample (up to 6 %) leads to the decrease in transition temperature to 900 °C and the increase in melting temperature to 1270 °C.[14] On the basis of gadolinium fluoride, the optimal annealing mode of the sample was selected. As a result of the experiment, it was found that the optimal conditions of REF_3 annealing are 5–7 min in a platinum crucible at 700 °C in an argon atmosphere.

The temperature and heat of melting of LaF_3 are comparable with the data obtained earlier by calorimetry[44,45] (Table 4). The melting point of LaF_3:Yb^{3+}, Ho^{3+} is significantly lower than that of LaF_3, which is consistent with the substitution of 15 % by more low-melting components than LaF_3 (T_{melt} = 1493 °C[14,45])", the melting temperature for YbF_3 is 1162 °C[44] and for HoF_3 is 1143 °C.[45] There are no extraneous reflexes on the DSC curves, and this fact confirms the formation of a solid solution, not a mixture of REF_3. For GdF_3:Yb^{3+}, Tm^{3+}, the change in melting temperature relative to GdF_3 is not significant (less than 15 °C) (Table 4), that is consistent with the nature of doped elements. The minimum deviation of the melting temperature of the solid solution from the pure compound is observed for YF_3:Yb^{3+}, Er^{3+}.

The melting peaks of LaF_3:Yb^{3+}, Ho^{3+} and GdF_3:Yb^{3+}, Tm^{3+} have a blurred form owing to the presence of a eutectic point or minimum in the ternary systems LaF_3 - YbF_3 - HoF_3 and GdF_3 - YbF_3 - TmF_3. The decrease in the melting enthalpy for samples REF_3:Yb^{3+}, RE'^{3+}confirms the formation of the solid solutions (Table 3).

LaF_3 does not have polymorphic transformation that is also observed for solid solution LaF_3:Yb^{3+}, Ho^{3+} (Figure 4). GdF_3 and YF_3 have polymorphic transformations and the transition temperatures indicated in Table 4. The polymorphic transition temperatures of GdF_3, YF_3 and solid solution REF_3:Yb^{3+}, RE'^{3+} are determined by extrapolating the line of peak slope and baseline. The enthalpies of the thermal effects of the polymorphic transformations are comparable with the literature values within the possible measurement error and the values are presented in Table 4.

The applicability of the obtained materials as biologic luminescent markers was tested by the observation of upconversion (UC) processes.[50–53] The low-power infrared laser diode with the central wavelength 976 nm was used for the excitation of UC luminescence. The wavelength of this laser is featured by the maximum penetration depth into biological tissues. At the same time, this wavelength is close to the resonant infrared transition of Yb^{3+} ion that is featured by the highest absorption coefficient among all f–f transitions of all rare earth ions. Excited Yb ions serve as the donors of the excitation that can be efficiently transmitted to the acceptor ions such as Er, Ho or Tm via energy transfer (ET). If the excitation energy of two or more donor ions is transferred to the same acceptor ion, then high-lying energy levels of acceptor will be excited, and luminescence from these levels will be emitted at the wavelengths lying in the visible or UV. The emitted radiation was detected by a waveguide-coupled Ocean Optics HR4000 spectrometer. The UC spectrum obtained from YF_3:Yb^{3+}, Er^{3+} sample is presented in Figure 5a.

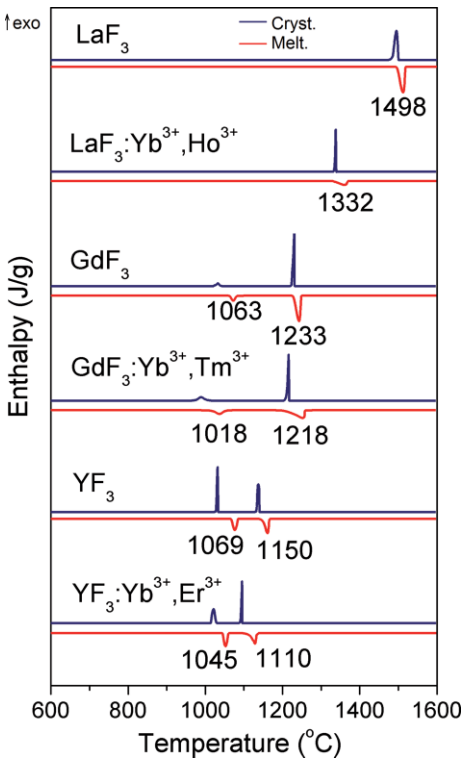

Figure 4. DSC curves.

The UC spectrum of YF_3:Yb^{3+}, Er^{3+} contains five distinctly detectable emission bands of Er.[54] Especial interest is the presence of $^4H_{9/2}$–$^4I_{15/2}$ transition that requires participation of at least three pump photons for the excitation of $^4H_{9/2}$ energy level. Another feature is complete domination of green

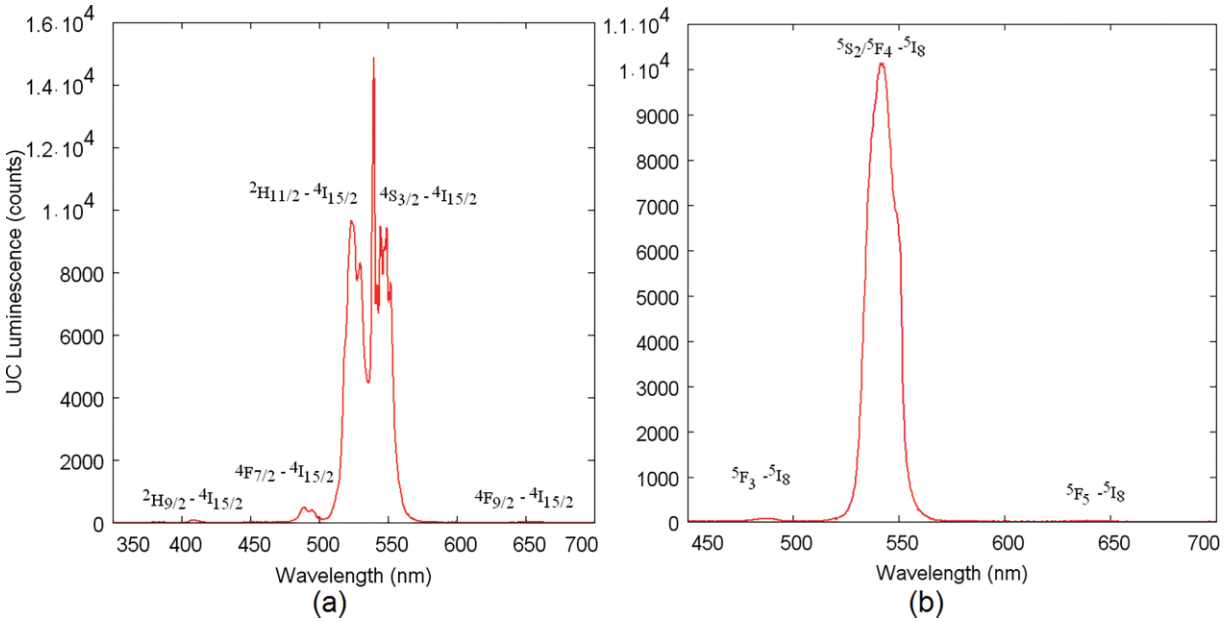

Figure 5. UC spectrum from (a) YF_3:Yb^{3+}, Er^{3+} and (b) LaF_3:Yb^{3+}, Ho^{3+} sample pumped at 976 nm.

($^2H_{11/2}$–$^4I_{15/2}$) and yellow-green ($^4S_{3/2}$–$^4I_{15/2}$) bands, being of approximately equal intensity, in contrast to, e.g., such fluoride UC material like $CsScF_4$:Er,Yb.[55] On the example of $^4S_{3/2}$–$^4I_{15/2}$ one can see that crystal-field split subcomponents of this band are spectrally well resolved, that evidences good crystallinity of the sample. The UC spectrum obtained from LaF_3:Yb^{3+}, Ho^{3+} sample is shown in Figure 5b.

In this case, three UC bands can be detected, as indicated in the spectrum. Yellow $^5S_2/^5F_4$–$^5I_8$ band is absolutely dominating over the red one, in contrast to e.g. upconverting molybdates,[56] Another feature is the prevalence of blue UC band over the red one. The UC luminescence in GdF_3:Yb^{3+}, Tm^{3+} was not detected in the conditions of our experiment. The energy level scheme of Tm ion differs from those of Ho and Er in the sense that for emerging of both blue and red UC luminescence, relatively higher-lying $^1G_4$ level must be reached by ET process, that requires three photons in the case of cascade UC process and two photons for cooperative process.[57] Therefore, the absence of UC luminescence in GdF_3:Yb^{3+}, Tm^{3+} can be ascribed to insufficient power of the pump source used.

Conclusions

The samples of solid solutions *RE*F_3:Yb^{3+}, *RE*′$^{3+}$ are synthesized in the following sequence of chemical transformations: thermal decomposition of a mixture of nitrates; sulfidation in the stream CS_2, H_2S; fluorination with hydrofluoric acid (4 % and 40 %). The product phase composition and the particle morphology are affected by the ionic radii of the rare earth elements.

The formation of solid solutions of *RE*F_3:Yb^{3+}, *RE*′$^{3+}$ is confirmed by the results of X-ray analysis, DSC and measured density. The temperatures of transitions and melting, and enthalpies of *RE*F_3 and solid solutions of *RE*F_3:Yb^{3+}, *RE*′$^{3+}$ were determined. The values obtained are commensurable with the literature data for compounds *RE*F_3. For *RE*F_3:Yb^{3+}, *RE*′$^{3+}$, the enthalpies of melting relative to *RE*F_3 decrease. It was established that the density of solid solutions are comparable to those calculated from the structure data (maximum error 4 %).

The particle morphology of LaF_3:Yb^{3+}, Ho^{3+} and GdF_3:Yb^{3+}, Tm^{3+} does not significantly depend on the concentration of hydrofluoric acid. The shape and size of the particles at different concentrations of HF do not change. A decrease in the concentration of HF (pH ≥ 3) leads to a slight preservation of sulfur atoms in the structure of the solid solution and does not allow obtaining a homogeneous product. The concentration of hydrofluoric acid significantly affects the reaction products with Y_2S_3:Yb^{3+}, Er^{3+}. The small size of the crystal radius of yttrium $r(Y^{3+}_{(CN\ 8)})$ = 1.159 Å[25] promotes the formation of the zeolite structure $(H_3O)Y_3F_{10}{\cdot}H_2O$: Yb^{3+}, Er^{3+}, which is formed in the presence of excedente of hydroxonium ions (at HF 30–40 %, pH ≤ 1.9). A further increase in the pH of the solution leads to a decrease in the content of hydroxonium ions and, as a consequence, the product of the reaction is only YF_3:Yb^{3+}, Er^{3+}. When heat treated at a temperature above 400 °C, the compound $(H_3O)Y_3F_{10}{\cdot}H_2O$: Yb^{3+}, Er^{3+} decomposes to YF_3:Yb^{3+}, Er^{3+}.

Acknowledgements

The authors would like to thank the staff of the Engineering Center of the Tyumen State University (special *Alexej V. Matigorov*) for their help in carrying out physical and chemical tests.

Keywords: Rare earth fluoride; Rare earth sulfide; Rare earth compounds; Solid solution; Upconversion

References

[1] T. E. Sukhanova, M. E. Vylegzhanina, S. V. Valueva, L. N. Borovikova, R. Yu. Smyslov, A. A. Kutin, K. I. Borygina, V. K. Adamchuk, M. L. Gelfond, *J. Surf. Invest. X-ray Synchotron. Neutron. Technol.* **2013**, *7*, 671–679.
[2] W. Ni, M. Li, J. Cui, Z. Xing, Z. Li, X. Wu, E. Song, M. Gong, W. Zhou, *Mater. Sci. Eng. C* **2017**, *81*, 252–260.
[3] S. A. Hilderbrand, F. Shao, C. Salthouse, U. Mahmood, R. Weissleder, *Chem. Commun.* **2009**, *28*, 4188–4190.
[4] T. Grzyb, M. Runowski, A. Szczeszak, S. Lis, *J. Phys. Chem. C* **2012**, *116*, 17188–17196.
[5] T. Grzyb, L. Mrowczynska, A. Szczeszak, Z. Sniadecki, M. Runowski, B. Idzikowski, S. Lis, *J. Nanopart. Res.* **2015**, *17*, 399 .
[6] Y. Liu, W. Chen, S. Wang, A. G. Joly, *Appl. Phys. Lett.* **2008**, *92*, 2835701–2835707.
[7] Y. Liu, W. Chen, S. Wang, A. G. Joly, S. Westocott, B. K. Woo, *Appl. Phys* **2008**, *103*, 063105.
[8] F. Tao, Z. Wang, L. Yao, W. Cai, X. Li, *J. Phys. Chem. C* **2007**, *111*, 3241–3245.
[9] D. Li, W. Yu, X. Dong, J. Wang, G. Liu, *J. Fluorine Chem.* **2013**, *145*, 70–76.
[10] A. Bensalah, M. Ito, Y. Guyot, C. Goutaudier, A. Jouini, A. Brenier, H. Sato, T. Fukuba, G. Boulon, *J. Lumin.* **2007**, *122–123*, 444–446.
[11] S. V. Kuznetsov, A. N. Kozlova, V. V. Voronov, D. V. Pominova, A. V. Ryabova, R. P. Ermakov, K. S. Gavrichev, A. E. Baranchikov, A. V. Khoroshilov, P. P. Fedorov, *Russ. J. Inorg. Chem.* **2018**, *63*, 293–302.
[12] S. Kuznetsov, Yu. Ermakova, V. Voronov, P. Fedorov, D. Busko, I. A. Howard, B. S. Richards, A. Turshatov, *J. Mater. Chem. C* **2018**, *6*, 598–604.
[13] P. P. Fedorov, B. P. Sobolev, *Cryst. Rep.* **1995**, *40*, 315–321.
[14] B. P. Sobolev, P. P. Fedorov, D. B. Steynberg, B. V. Sinitsyn, G. S. Shakhkalanian, *J. Solid State Chem.* **1976**, *17*, 191–199.
[15] P. P. Fedorov, M. V. Nazarkin, R. M. Zakalyukin, *Cryst. Rep.* **2002**, *47*, 281–286.
[16] B. P. Sobolev, P. P. Fedorov, K. B. Seiranyan, N. L. Tkachenko, *J. Solid State Chem.* **1976**, *17*, 201–212.
[17] P. P. Fedorov, N. I. Sorokin, *Inorg. Mater.* **2017**, *53*, 1307–1311.
[18] J.-J. Maguer, M. P. Crosnier-Lopez, G. Courbion, *J. Solid State Chem.* **1997**, *128*, 42–51.
[19] G. Corbel, G. Courbion, F. L. Berre, M. Leblanc, J.-M. L. Meins, V. Maisonneuve, N. Mercier, *J. Fluorine Chem.* **2001**, *107*, 193–198.
[20] J.-J. Maguer, G. Courbion, *J. Solid State Chem.* **1997**, *128*, 52–61.
[21] F. L. Berre, E. Boucher, M. Allain, G. Courbion, *J. Mater. Chem.* **2000**, *10*, 2578–2586.
[22] M. N. Mayakova, A. A. Luginina, S. V. Kuznetsov, V. V. Voronov, R. P. Ermakov, A. E. Baranchikov, V. K. Ivanov, O. V. Karban, P. P. Fedorov, *Mendeleev Commun.* **2014**, *24*, 360–362.
[23] P. P. Fedorov, M. N. Mayakova, S. V. Kuznetsov, V. V. Voronov, R. P. Ermakov, K. S. Samarina, A. I. Popov, V. V. Osiko, *Mater. Res. Bull.* **2012**, *47*, 1794–1799.
[24] B. E.-G. Lucier, K. E. Johnston, D. C. Arnold, J.-L. Lemyre, A. Beaupre, M. Blanchette, A. M. Ritcey, R. W. Schurko, *J. Phys. Chem. C* **2014**, *118*, 1213–1228.
[25] R. D. Shannon, *Acta Crystallogr., Sect. A* **1976**, *32*, 751–767.
[26] [1].-P. Jia, Q. Zhang, B. Yan, *Mater. Res. Bull.* **2012**, *47*, 3301–3307.
[27] N. F. Stephens, P. Lightfoot, *J. Solid State Chem.* **2007**, *180*, 260–264.
[28] M. N. Mayakova, S. V. Kuznetsov, V. V. Voronov, A. E. Baranchikov, V. K. Ivanov, P. P. Fedorov, *J. Inorg. Chem.* **2014**, *59*, 773–777.
[29] L. R. Batsanova, *Russ. Chem. Rev.* **1971**, *40*, 945–979.
[30] X. Li, S. Gai, C. Li, D. Wang, N. Niu, F. He, P. Yang, *Inorg. Chem.* **2012**, *51*, 3963–3971.
[31] M. Runowski, S. Lis, *J. Alloys Compd.* **2016**, *661*, 182–189.
[32] B. Richard, J.-L. Lemyre, A. M. Ritcey, *Langmuir* **2017**, *33*, 4748–4757.
[33] C. Peng, C. Li, G. Li, S. Li, J. Lin, *Dalton Trans.* **2012**, *41*, 8660–8668.
[34] J.-L. Lemyre, A. M. Ritcey, *Chem. Mater.* **2005**, *17*, 3040–3043.
[35] C. Li, P. Ma, P. Yang, Z. Xu, G. Li, D. Yang, C. Peng, J. Lin, *CrystEngComm* **2011**, *13*, 1003–1013.
[36] P. P. Fedorov, A. A. Luginina, S. V. Kuznetsov, V. V. Osiko, *J. Fluorine Chem.* **2011**, *132*, 1012–1039.
[37] L. Schmidt, *Synthese und Charakterisierung von nano-SrF_2 und -YbF_3 für Anwendungen in der Dentalmedizin*, Dr. rer. nat. Thesis, Berlin, 2015, 155.
[38] A. Tressaud, K. R. Poeppelmeier, *Photonic and Electronic Properties of Fluoride Materials. Progress in Fluorine Science Series*, Elsevier, 2016, p. 513.
[39] I. A. Razumkova, A. N. Boiko, O. V. Andreev, A. S. Basova, *Russ. J. Inorg. Chem.* **2017**, *62*, 418–422.
[40] O. V. Andreev, I. A. Razumkova, O. V. Boiko, *J. Fluorine Chem.* **2018**, *207*, 77–83.
[41] I. A. Razumkova, *J. Fluorine Chem.* **2018**, *205*, 1–4.
[42] S. V. Kuznetsov, V. V. Osiko, E. A. Tkatchenko, P. P. Fedorov, *Russ. Chem. Rev.* **2006**, *75*, 1065–1082.
[43] B. P. Sobolev, *The Rare Earth Trifluorides, Part 1*, Institut d'Estudis Catalans, Barcelona, 2000, p. 530.
[44] F. H. Spedding, B. J. Beaudry, D. C. Henderson, J. Moorman, *J. Chem. Phys.* **1974**, *60*, 1578–1588.
[45] F. H. Spedding, D. C. Henderson, *J. Chem. Phys.* **1971**, *54*, 2476–2483.
[46] O. V. Andreev, O. Yu. Mitroshin, I. A. Razumkova, *Russ. J. Inorg. Chem.* **2008**, *53*, 323–326.
[47] O. V. Andreev, O. Yu. Mitroshin, I. A. Razumkova, *Russ. J. Inorg. Chem.* **2007**, *52*, 1161–1164.
[48] N. F. Stephens, P. Lightfoot, *J. Solid State Sci.* **2006**, *8*, 197–202.
[49] A. Grzechnik, W. A. Crichton, J. Y. Gesland, *J. Solid State Sci.* **2003**, *5*, 757–764.
[50] C. S. Lim, A. S. Aleksandrovsky, M. S. Molokeev, A. S. Oreshonkov, V. V. Atuchin, *J. Solid State Chem.* **2015**, *228*, 160–166.
[51] C. S. Lim, *Mater. Res. Bull.* **2016**, *75*, 211–216.
[52] L. Jiang, G. Liu, D. Li, X. Dong, W. Yu, *Spectrochim. Acta Part A* **2018**, *201*, 88–97.
[53] M. Runowski, N. Stopikowska, D. Szeremeta, S. Goderski, M. Skwierczynska, S. Lis, *ACS Appl. Mater. Interfaces* **2019**, *11*, 13389–13396.
[54] C. S. Lim, A. S. Aleksandrovsky, M. S. Molokeev, A. S. Oreshonkov, D. A. Ikonnikov, V. V. Atuchin, *Dalton Trans.* **2016**, *45*, 15541–15551.
[55] D. A. Ikonnikov, V. N. Voronov, M. S. Molokeev, A. S. Aleksandrovsky, *Opt. Mater.* **2016**, *60*, 584–589.
[56] Ch. S. Lim, V. V. Atuchin, A. S. Aleksandrovsky, M. S. Molokeev, A. Oreshonkov, *J. Alloys Compd.* **2017**, *695*, 737–746.
[57] A. S. Aleksandrovsky, I. Gudim, A. S. Krylov, A. Malakhovskii, V. L. Temerov,16210 *J. Alloys Compd.* **2010**, *496*, L18-L21.

Received: August 24, 2019
Published Online: ■

Journal of Inorganic and General Chemistry
ZAAC
Zeitschrift für anorganische und allgemeine Chemie

ARTICLE